

Quantum Embedding Search for Quantum Machine Learning

Nam Nguyen, *Student Member, IEEE*, and Kwang-Chen Chen, *Fellow, IEEE*

Abstract—This paper introduces a novel quantum embedding search algorithm (QES, pronounced as “quest”), enabling search for optimal quantum embedding design for a specific dataset of interest. First, we establish the connection between the structures of quantum embedding and the representations of directed multi-graphs, enabling a well-defined search space. Second, we instigate the entanglement level to reduce the cardinality of the search space to a feasible size for practical implementations. Finally, we mitigate the cost of evaluating the true loss function by using surrogate models via sequential model-based optimization. We demonstrate the feasibility of our proposed approach on synthesis and Iris datasets, which empirically shows that found quantum embedding architecture by QES outperforms manual designs whereas achieving comparable performance to classical machine learning models.

Index Terms—Quantum Embeddings, Quantum Machine Learning, Automated architecture search, Sequential model-based optimization..

1 INTRODUCTION

Quantum machine learning is a potential advancement of quantum computing in the Noisy Intermediate-Scale Quantum (NISQ) era. As the validity of near-term quantum devices, quantum machine learning poses exciting advantages over classical counterparts. The potential quantum advantage can be addressed based on the geometric test over the input data space, followed by the complexity test for specific functions [1]. Although quantum machine learning models are more often than not referred to as quantum neural networks, the terminology is misleading to some extent. The classical neural networks can transform the original data space into higher or lower dimensional space based on the design of neural architectures. For example, state-of-the-art neural architectures tend to transform high-dimensional inputs such as images or sequences into lower-dimensional representations of latent vectors. In contrast, quantum neural networks possess a similar mathematical structure to kernel methods, where input data is embedded into high-dimensional quantum Hilbert space [2], [3], [4]. The quantum representations of input data are the outcome of quantum embedding, which plays a crucial role in the performance of quantum classifiers [5]. Such quantum embeddings are quantum model functions, referred to as parameterized quantum circuits [6], quantum neural networks [7], [8], or variational circuits [9], [10]. The quantum embeddings are often manually designed for specific use-cases, which requires extensive expert knowledge and computational expense.

This paper introduces a quantum embedding search algorithm, an automated search framework to find optimal quantum embedding architecture for data-specific scenarios. We summarized the contribution of QES as follows:

- 1) We instigate an efficient encoding scheme of quantum embedding’s architectures as directed multi-graphs, which enable us to well-define the search space of the

quantum embedding search problem. Moreover, we introduce the constraints over the search space by entanglement level, which reduces the cardinality of the search space to a reasonable size for practical implementations.

- 2) We leverage the sequential model-based optimization via Tree Parzen Estimator [11] (SMBO-TPE). The advantage of our search strategy is two-fold: (1) usage of surrogate models enables the approximation of the actual loss function, which significantly reduces computational cost in the optimization, and (2) non-parametric densities in TPE allows us to draw multiple architecture candidates for evaluating the expected improvement of surrogates, which is more computationally effective.
- 3) Discovered quantum embedding architectures by QES outperform manual design in both synthesis and Iris dataset [12] while achieving compatible results compared to classical machine learning models.

We organize the paper as: Section 2 summarizes related work in the literature, Section 3 discusses our proposed QES algorithm in-depth, Section 4 reports experimental results. Finally, we discuss the implication and thread to the validity of QES in Section 5.

2 RELATED WORKS

2.1 Automated Architecture Search

Automated architecture search has drawn significant attention from the ML/DL-related research community. The motivation of the research branch is practical but straightforward; that is, there is no universal design of neural architecture for all datasets. The main objective of such an algorithm is to find an optimal design for the model’s architectures based on pre-defined selection criteria. Initialization of automated architecture search algorithm starts with defining the configuration of the search space. The basic search space structure is known as flat search space, referred to as hyper-parameters optimization. For example, the flat search space of neural architecture search is to find the depth (number of layers), the width (number of initial channels), and kernel

• M. The authors are with the Department of Electrical Engineering, University of South Florida, Tampa, FL 33620.
E-mail: namnguyen2@usf.edu

sizes. A more complicated formation of search space is cell-based neural architectures, where each neural candidate can be encoded as a directed acyclic graph [13], [14]. The search space of our proposed QES is motivated by the latter configuration, which will be discussed hereafter in Section 3. Many frameworks have been proposed to tackle the automated architecture search problems. An early solution involves random search [15], which is often used as the baseline for comparison. The next progression is the development of sequential model-based optimizations, which mitigate the expensive cost of actual loss function by using surrogate models [11], [16]. More advanced search strategies have been proposed to tackle the problem, involving reinforcement learning [13], evolutionary [17], gradient-based with continuous relaxation and bilevel optimization [18], heuristic search with performance prediction [19] and SMBO-TPE [20]. The biggest challenge in automated architecture search is the computational cost for the search phase. Search strategies such as reinforcement learning and evolutionary take up to 2000 – 3150 GPU days to find optimal architecture for the CIFAR-10 dataset [13], [14]. Although progression helps to shorten the time complexity of the search procedure to reasonable time and hardware, the expensive computation is inherited from the costly evaluation of the cost function. The same issue appears when training quantum machine learning models in near-term quantum computers and quantum simulators. Recent work solves quantum circuit optimization problems by reinforcement learning with circuit transformation [21], which achieve remarkable results. However, such an algorithm still relies on evaluating the true loss function for maximizing the cumulative reward. We find that sequential model-based optimization is another potential solution for quantum embedding search/quantum circuit optimization since the approximation of true loss function by surrogates reduces the computational expense of searching for the optimal quantum embedding architecture.

2.2 Quantum Machine Learning

Quantum machine learning has become an emerging sub-discipline of quantum computing due to its potential application for near-term intermediate-scale quantum hardware. Current literature has witnessed the advantages of quantum machine learning over its classical competitors, which involve various learning tasks [22], [23], [24], [25], [26], [27]. The dominant approach for quantum machine learning is circuit-based models, referred to as variational quantum classifiers [9], [10], [28]. Different strategies of classifier in the quantum Hilbert space have been proposed, including linear classifier [29], bitstrings parity-binary mapping [30], Helstrom, and fidelity classifiers [5]. Moreover, a strong connection between quantum machine learning and kernel methods has been established in [2], [3], [4]. The core component of circuit-based quantum machine learning models is the variational (parameterized) circuits called ansatz (plural ansätze). The construction of an ansatz is formed by stacking multiple identical sub-layers, similar to the construction of cell-based neural architecture designs [13]. Although many variational ansätze have been proposed in the literature [4], [7], [28], [31], [32], [33], [34], [35], [36], [37], [38], [39], [40], [41], there is no general framework to design optimal ansatz for data-specific scenarios or specific use-cases. It is the main motivation for our QES algorithm, which directly tackles the problem of discovering optimal quantum embedding architectures for given datasets of interest.

3 QUANTUM CIRCUIT EMBEDDING SEARCH

3.1 Quantum Embeddings

Let $\mathbf{x} \in \mathcal{X}$ be the feature vector in classical data space, quantum embedding is similar to kernel method since the input feature space is mapped to a high-dimensional Hilbert space [2]. Mathematically speaking, the mapping is given by

$$\begin{aligned} \mathcal{X} &\rightarrow \mathcal{H} \\ \mathbf{x} &\rightarrow |\phi(\mathbf{x})\rangle, \end{aligned} \quad (1)$$

where $\phi(\mathbf{x})$ is the *quantum representations* of original input data and \mathcal{H} is the quantum Hilbert space. In particular, a system of n qubits is corresponding to a vector space \mathbb{C}^{2^n} . The measurements on these quantum states yield embedded outputs, that is the representation of the observable in the latent space. In general, the intermediate representations of a quantum state can be written as

$$g(\mathbf{x}) = \langle \mathbf{x} | \mathcal{Z} | \mathbf{x} \rangle, \quad (2)$$

where \mathcal{Z} is the measurement associated with the observable. Our choice for \mathcal{Z} is the expectation values in \mathbb{Z} basis over all qubits, which is $\mathcal{Z} = \prod_{i=1}^n \sigma_z$. State-of-the-art quantum machine learning model [2], [5] transforms the expectation in continuous domain to categorical labels by thresholding the outcome. In contrast, we leverage the continuous latent representation of the measurements. The decision boundary of the quantum machine learning model in Figure 1 is created by single-layer linear classifier. We will show the power of representation learning from quantum embeddings over classical counterparts with five-time complexity hereafter in Section 4.

3.2 Ansatz Circuit

The structure of a quantum embedding includes a stack of multiple circuit ansatz (Figure 1) which results in intractable latent representations for universal quantum computing [42]. The Quantum Approximate Optimization Algorithm (QAOA) [28] inspires the embedding circuit ansatz, which enables the transformation of classical input data into quantum representations. Figure 1 shows our assumption for the design of a partially parameterized circuit ansatz, which includes an input-depend unitary block, fixed unitary block and learnable unitary block. Primitive gates of unitary includes Control-rotation gates $R_{\sigma_1 \in \{X, Y, Z\}}(\mathbf{x})$, which are parameterized by the input data \mathbf{x} . Then immediate quantum representations $U_1 |\phi(\mathbf{x})\rangle$ are fed forward into the fixed unitary block including multiple entangling patterns active on certain number of qubits. The primitive gates for entanglement establishment is CNOT gate, which offer a highly entangled state over all qubits in the system. Moreover, CZ gates can be made by CNOT gates for entangling patterns, which is introduced in [43] to tackle the vanishing gradients problem (barren plateaus). Finally, the last block of an ansatz circuit includes control rotation gates $R_{\sigma_2 \in \{X, Y, Z\}}(\mathbf{w})$ parameterized by learnable weights \mathbf{w} . Mathematically, the ansatz acts on n -qubits system as

$$|\mathbf{x}\rangle \rightarrow \Psi(\mathbf{x}, \mathbf{w}) |0\rangle^{\otimes n}, \quad (3)$$

where $\Psi(\mathbf{x}, \mathbf{w})$ is parameterized unitary transformation of \mathbf{w} with realizations \mathbf{x} . By backpropagation, the set of weights \mathbf{w} will be learned to minimize the cost function throughout the training process. Figure 3 depicts several manual designs for strongly entangled patterns of an quantum embeddings, which will be considered as baseline comparison for Section 4.

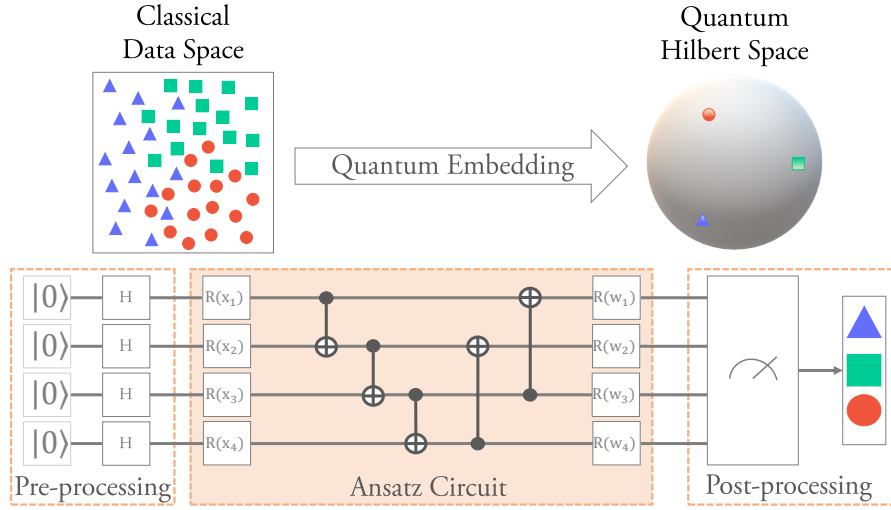


Fig. 1: (Top) **Quantum embeddings for supervised quantum machine learning.** Similar to kernel methods, quantum embedding transforms observations in classical data space into quantum Hilbert space of quantum states, which the inner product of quantum representations can represent. (Bottom) **Architecture of a quantum machine learning model formed by selected set of quantum circuits.** The ansatz circuit plays an crucial role in the circuit model, enabling learning model's weights w accordingly to input data x .

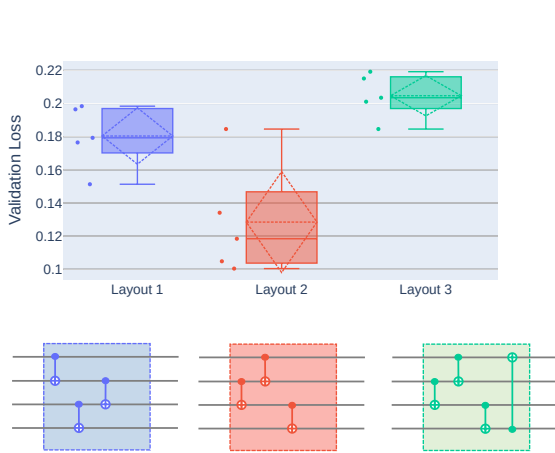


Fig. 2: **Preliminary results of quantum embeddings with different entangling structures on Iris dataset.** The permutation of CNOT gates leads to significant improvement in terms of validation loss. Moreover, extending the number of CNOT gates may reduce the performance of the embedding.

Observations Before further discussion, we would like to address several findings from our observations over the preliminary experiments (Figure 2).

- 1) Different entangling structures result in varying loss values in the validation set.
- 2) Entangling structure is permutation variant. In other words, the order of CNOT gates over qubits significantly impacts the overall performance.
- 3) Larger number of CNOT gates does not guarantee higher predictive power of the resulting architecture.
- 4) Repetitions of similar entangling connections are possible.

The detail of preliminary experiments on the Iris dataset is given in

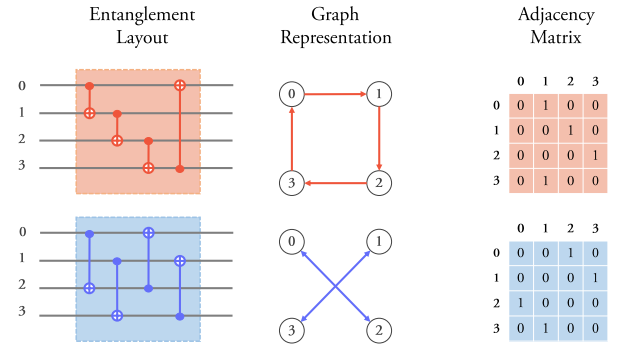


Fig. 3: **Directed multi-graph representation for given entangling structures.** The representation of corresponding graphs are also represented as adjacency matrices, where diagonal entries are 0 and off-diagonal elements takes value 0 (absence of CNOT gate) or 1 (presence of CNOT gate). Moreover, these hand-crafted designs are referred as baseline 1 and baseline 2, respectively.

Section 6.2, where several statistical tests are conducted to provide statistical evidence for our observations.

3.3 Search Space Configuration

3.3.1 Encoding Scheme

We proposed a representation for entangling layouts as directed multi-graphs, in which vertices represent qubits and edges formed by CNOT gates. The main objective of our proposed work is to find the optimal structure for entangling patterns on a given dataset. Hence, we fix the choice of rotation axis in the first and third parameterized unitary blocks at $\sigma_1 = \sigma_2 = Y$ [5]. In other words, we only consider parameterized control rotation by Y-axis over all qubits. Moreover, the encoded graph representation for each candidate circuit layout in the search space is associated with an asymmetric adjacency matrix (Figure 3), which allows better illustration in the search space complexity analysis.

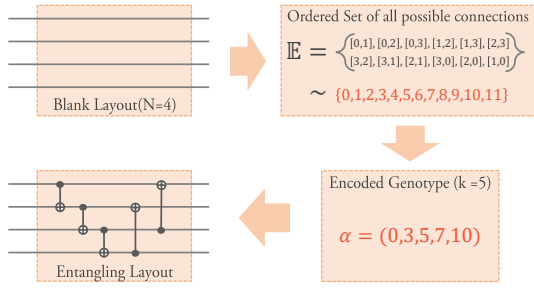


Fig. 4: **Encoding scheme for the search generator.** First, the set of all possible edges is generated considering order of elements. Then "genotype" vector of length k is drawn by the search engine, in which elements are index of corresponding edges.

3.3.2 Complexity Analysis

Given a set of N qubits, the number of off-diagonal entries for the adjacent matrix is given as

$$E = N^2 - N = N(N - 1) \quad (4)$$

With regard the order permutation of CNOT gates in candidate circuit layouts, the total number of possible candidate in the search space of N qubits embeddings is

$$|\Omega_{\text{Full}}| = \sum_{k=0}^E k! \binom{E}{k} = \sum_{k=0}^E \frac{E!}{(E-k)!}. \quad (5)$$

As a result, the search space of all possible circuit layouts is extensively large ($\approx 1.3 \times 10^9$) even though we only consider a small system of 4 qubits. Moreover, the complexity of the search space is exponentially expanded when increasing the number of input qubits, which is tremendously hard to find the optimal circuit layout for the entanglement block. Thus, we proposed additional parameters for the search space configuration, called the entanglement level, which is set to be the fixed number of CNOT gates within the entangling layer. Given a pre-defined entangling level k , the total number of possible circuit candidates in the reduced search space is:

$$|\Omega_{\text{Reduced}}| = k! \binom{E}{k} = \frac{E!}{(E-k)!}. \quad (6)$$

By implementing the proposed entangling level, the search space is reduced to a reasonable cardinality for finding optimal circuit architecture. Together with proposed encoding scheme (Figure 4), each circuit candidate in the search space of N qubits constrained by entangling lever k is represent by an encoded genotype vector α of length k , whose each component is corresponding with each element of the ordered set of all possible connection $\mathcal{E} = \{e_i\}_{i \in \{0, \dots, E\}}$.

3.4 Sequential Model-based Optimization

Figure 5 illustrates the general framework of quantum circuit embedding search. We employ the sequential model-based optimization (SMBO) using tree Parzen estimator [11] as the search strategy for the optimal circuit candidate, which can be mathematically stated as

$$\alpha^* = \arg \min_{\alpha \in \Omega} \mathcal{L}_{\text{val}}^{(\alpha)}(\mathbf{y}, \hat{\mathbf{y}}) \quad (7)$$

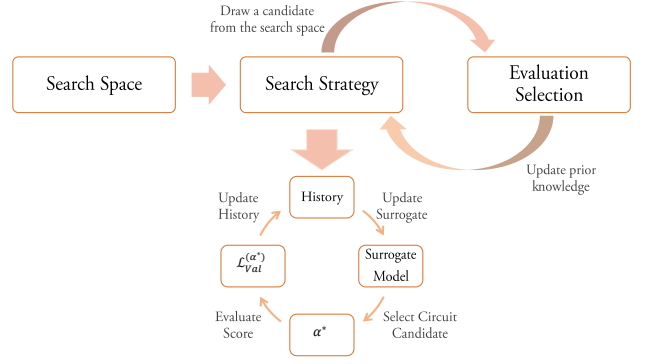


Fig. 5: **General framework of automated model search.** After well-defining the search space, the automated intelligence draws an architecture candidate following search strategy. The drawn architecture will be evaluated using selection criteria, which create response for updating the search intelligence. In investigating search strategy SMBO-TPE, the prior knowledge of search intelligence will be updated corresponding to response score during the search phase.

Algorithm 1 Sequential Model-based Optimization via TPE estimator

Given $\Omega, \mathcal{L}(\cdot), M_0, T, S(\cdot)$ and history \mathcal{H}

initialize $\mathcal{H} \leftarrow \emptyset$

for $i = 1$ to number of trials T :

$\alpha^* \leftarrow \arg \min_{\alpha} S(\alpha, M_{i-1})$

compute $\mathcal{L}_{\text{val}}^{(\alpha^*)}(\mathbf{y}, \hat{\mathbf{y}})$

update $\mathcal{H} \leftarrow \mathcal{H} \cup \{\alpha^*, \mathcal{L}_{\text{val}}^{(\alpha^*)}(\mathbf{y}, \hat{\mathbf{y}})\}$

fit M_i to \mathcal{H}

return \mathcal{H}

The cost function $\mathcal{L}_{\text{val}}^{(\alpha)}(\mathbf{y}, \hat{\mathbf{y}})$ is the validation loss value corresponding to the circuit candidate α , which is modeled by less computational expensive surrogate model $S(\cdot)$ by SMBO. In Algorithm 1, we aim to optimize the Expected Improvement (EI) at each iteration of the optimization. Given a threshold \bar{t} , the EI is given by

$$\text{EI}_{\bar{t}} = \int_{-\infty}^{\infty} \max(\bar{t} - t) p_M(t|\alpha) dt, \quad (8)$$

where M is an arbitrary model that $\mathcal{L}_{\text{val}}^{(\alpha)}(\mathbf{y}, \hat{\mathbf{y}})$ will exceed \bar{t} . The TPE estimator enables the decomposition of the conditional probability $p(t|\alpha)$ as two densities:

$$p(\alpha|t) = \begin{cases} l(\alpha) & \text{if } t < \bar{t} \\ g(\alpha) & \text{if } t \geq \bar{t} \end{cases}, \quad (9)$$

reforming the EI in Equation 8 into

$$\begin{aligned} \text{EI}_{\bar{t}} &= \int_{-\infty}^{\bar{t}} (\bar{t} - t) \frac{p(\alpha|t)p(t)}{p(\alpha)} dt \\ &\propto \left[p(t < \bar{t}) + \frac{g(\alpha)}{l(\alpha)} [1 - p(t < \bar{t})] \right]^{-1} \end{aligned} \quad (10)$$

Due to the decomposition, the TPE estimator enables sampling multiple candidates based on the density $l(\cdot)$, allowing more efficient estimation of the EI.

3.5 Selection Criteria

Evaluating the effectiveness of quantum embeddings means determining its power of representations learning. The quantum embedding aims to learn abstract patterns from input data, whose distributions are variant and highly correlated. Exemplary quantum representations possess a high level of generalization, which means reasonable-sized learned embedded representations can capture overall concepts from a massive number of inputs. Moreover, good quantum representations need to mitigate the variance in the input data distribution and disentangle the factor of variation [44]. The evaluation criteria of representations learning ability are distinguishable from the evaluation of any machine learning algorithms. For example, the objective of the training machine learning model is clear, in which we aim to minimize the number of misclassified instances (classification) or errors between predicted and actual values (regression). On the other hand, the objective of representation learning remains open and depends on how we adapt it to training criteria. In the scope of this paper, we assume a realistic and straightforward assumption: the optimal quantum embedding results in the best validation accuracy, i.e., minimizing the loss value in the validation set. The evaluation can be done by linear evaluation protocol [45], [46], which is commonly used in self-supervised/self-training literature. In the protocol, we only append an additional linear layer to the embedding, depending on the number of predicted classes. Thus, the final performance of models can be entirely attributed to the embedding architecture, i.e., more powerful embeddings achieve higher validation scores.

4 NUMERICAL EXPERIMENTS

We illustrate our proposed QES using synthesis and benchmark Iris dataset. The generated dataset includes 400 observations in the feature space of dimension 4, which involves the classification of three classes. We employ a small factor of hypercube size to obtain a synthesis dataset that is hard to be separated. By doing so, we can evaluate the magnitude of improvement from our discovered circuit embedding in comparison to classical machine learning, which is support vector machine, extreme gradient boosting, and fully connected neural network. Moreover, we report the hyper-parameter setting for generating synthesis dataset in Section, enables reproducing of our work for practitioners. Besides, the detailed hyper-parameter setting for training the quantum embeddings is given in Appendix 6.1. Regarding the benchmark dataset, we consider the Iris dataset to illustrate our proposed QES algorithms' effectiveness compared to state-of-the-art quantum embedding designs.

4.1 Results on Synthesis Data

In the search phase on synthesis dataset, we consider two search spaces corresponding with $k = 4$ and $k = 8$. Moreover, the depth of each architecture candidate is set equal to two layers during both search phase and evaluation phase. Figure 6 illustrates the found architectures using SMBO-TPE and baseline random search. It worth mentioning that the model complexity of the two setting is equivalent, that number of parameters in derived embedding architectures are equal. It is because the primitive CNOT gates does not contain any learnable weights. The score function for both of search procedure is based on the loss value on the (independent) validation set. We compare our found architectures with two

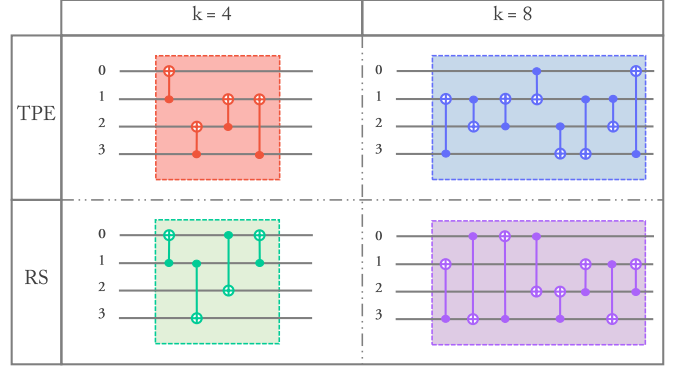


Fig. 6: **Discovered quantum circuit architectures from different search space configurations and search strategies.** Found architecture contains a sequence of CNOT gates, which establishing entanglement over all qubits.

common baseline entangling structures (strongly entangled layers) in Figure 3 and also with classical machine learning counterparts. In Table 1, our discovered quantum embedding circuit under gains a significant improvement in comparison to the baseline structures, while nearly achieve the performance of SVM and XGBoost with only minimal gap of 0.5%. Moreover, a large improvement of over 10% gain in validation accuracy is witnessed in comparison with neural network with the same number of parameters. Besides, expanding the search space to $k = 8$ enables discovering circuit structures with higher predictive power, consistently for both search strategies.

We further analyze the effectiveness of SMBO-TPE compared to baseline random search. Figure 7 shows the intermediate values of search strategy over trials of the two investigating optimization approaches. Overall, the validation loss converges after 50 epochs for both settings of the search space. Moreover, optimal architectures are found in early trials using SMBO-TPE, while random search discovers such architectures in late trials of the search phase. Another advantage of SMBO-TPE over random

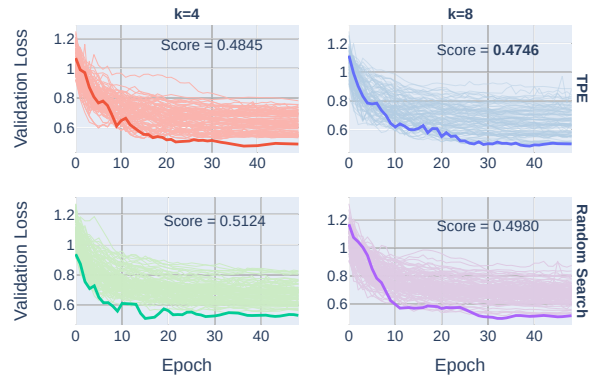


Fig. 7: **Training response of all trials under each search space configurations and search strategies on synthesis dataset.** Each architecture candidate is trained for 100 epochs at each trial. The validation loss converges within 50 epochs (as shown). Best score is witnessed from the search space with $k = 8$ under SBMO-TPE.

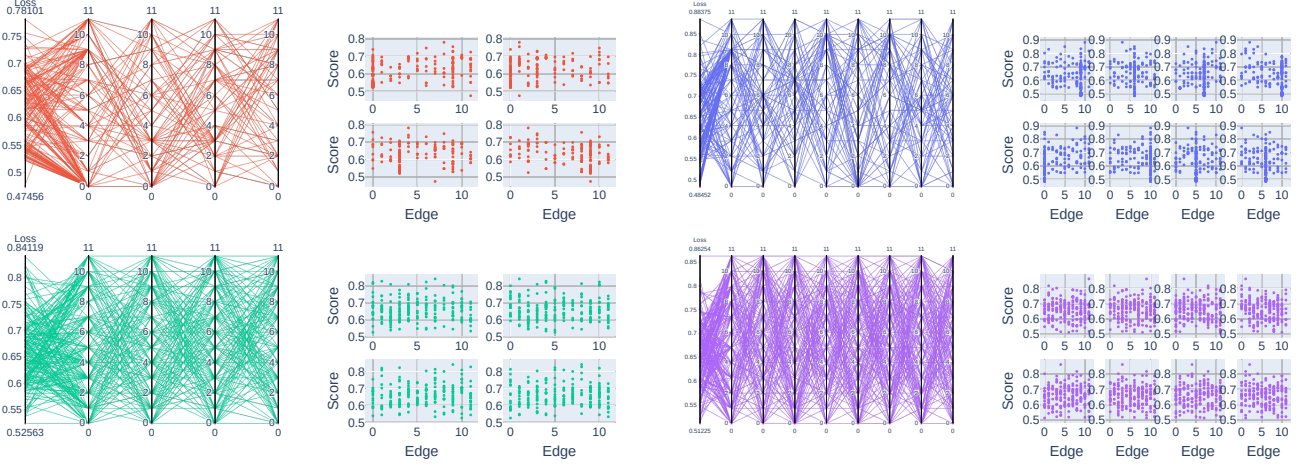


Fig. 8: **Parallel coordinates plot of parameters in the search space.** SBMO-TPE concentrates on edges that potentially leads to higher expected improvement, resulting in denser parameter’s landscape. On the other hand, the sampled edges by random search are widely spread out throughout the landscape.

Model	Accuracy (%)	Search Cost (GPU days)
Neural Network (fair)	71.00	-
SVM (ovo) [47]	84.00	-
XGBoost [48]	83.50	-
Entangling Baseline 1	74.00	-
Entangling Baseline 2	81.00	-
QES-RS ($k = 4$)	79.00	2
QES-RS ($k = 8$)	81.25	4
QES-TPE ($k = 4$)	82.00	2
QES-TPE ($k = 8$)	83.50	4

TABLE 1: **Comparison of found architectures with classical machine learning models and baseline hand-crafted entangling structure on synthesis dataset.** The evaluation is the validation accuracy based on 5 independent runs. Discovered quantum embedding outperforms baseline designs while achieves compatible performance as classical machine learning models.

search is depicted in the parallel coordinate plot, where we can see that the TPE sampler leverages knowledge during the search phase to update its prior knowledge. Sampling results from TPE concentrate on edges that potentially form higher predictive performance, while the random search’s sampled edges are widely spread throughout the configuration space.

Finally, the search cost of quantum embeddings is significantly higher than searching for classical neural network architectures due to the computational limitation of near-term quantum simulators. For example, candidates in neural architecture search are convolution neural networks involving up to millions of parameters, which can be found in only $0.25 - 8$ GPU days by recent state-of-the-art NAS algorithms [18], [20]. On the other hand, training a minor quantum embedding of very few qubits consumes much larger computational expenses. Our experimental setting takes $2 - 4$ GPU days to search for an architecture of only 23 parameters on the quantum simulators. The cost may be even expanded when we consider mid-to large-scale datasets. Fortunately, the computational expenses are majorly accounted for training the quantum embeddings. In other words, the enhancement of

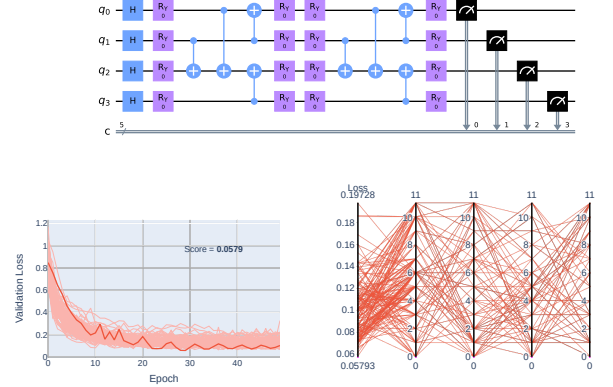


Fig. 9: **Found architecture of quantum embedding and its optimization history.** The same pattern is as presented on simulated dataset. The full architecture of the quantum embedding includes stack of two identical layers.

quantum computing/quantum machine learning in the near-term device will directly benefit the effectiveness of our proposed QES.

4.2 Results on Iris dataset

The construction of the search space on the Iris dataset only considers the entangling level of $k = 4$. We present the complete architecture of quantum embedding in Figure 9, which involves a stack of two identical found architectures in the search phase. The same pattern in the simulated dataset, where the TPE sampler leverages the knowledge learned from response scores to update its prior distribution, enables better architectures. The discovered architecture achieves 95.33 ± 0.0125 in the validation accuracy (based on ten independent runs), outperforming two baseline designs close to 2%. It worth highlighted that the found architecture reaches the consistent performance of a fully connected neural network with almost $5 \times$ the number of parameters (single layer with ten hidden nodes). It indicates more effectiveness of representations on quantum Hilbert space over classical data space since the quantum embedding only contains 8 learnable

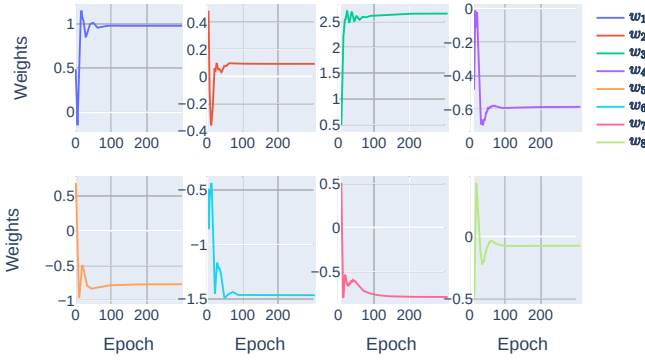


Fig. 10: Learning curves of quantum embedding's parameters on Iris dataset. Model weights start converging after 100 epochs, achieve 95.33 ± 0.0125 in validation accuracy.

parameters compared to 94 parameters in fair neural network embedding. Moreover, the weights of variational quantum embedding converge after 100 epochs on the Iris dataset, remaining the same in subsequent epochs as shown in Figure 10.

We also witness that the Iris dataset contains very well-representation observations, which can be easily separated. Hence, the magnitude of validation loss is hard to capture. On the other hand, we generated the synthesis data with slight class separation, which is more challenging to classify. As a result, we can observe the magnitude of validation loss from different quantum embedding designs.

5 DISCUSSION

5.1 Implication

Beyond the numerical experiments, we would like to address several general principles from our QES. First, our proposed approach provides an automated search intelligence that can find an optimal architecture of a quantum embedding circuit for a given dataset. It is reasonable to believe that there is no universal design of the embedding structure for every dataset, but instead, we can derive optimal architectures that well-performs on the dataset.

5.2 Threads to Validity

Threats to the internal validity of QES consider the reproducibility of the algorithm, which is the most challenging factor in automated machine learning [49], [50]. As we are in the noisy intermediate-scale quantum era, such issues have been amplified compared to classical computational hardware. Moreover, our proposed QES relies on the assumption of the entangling level that tremendously reduces the cardinal of the search space. Hence, we lack empirical evidence of the effectiveness of QES on expanded search space, especially when the number of qubits is scaled. We want to defer the investigation of such a problem for further study. Nevertheless, QES well-performs in small qubits can achieve similar results with classical machine learning counterparts and outperform basic entangling structures.

Threats to external validity include the generalization of QES on different data scenarios, the number of qubits in the system,

and noises inherited from actual quantum computing hardware. Although the experimental results from simulated quantum computing hardware are robust and stable, the story may change when we implemented QES on near-term noisy quantum computers. Another thread is the computational limitation of near-term quantum computers and quantum simulators. The cost for training single quantum embedding is remarkably higher than training classical encoders in the quantum simulations, which leads to a very high computational expense for the search phase.

6 CONCLUSION

This paper proposes an automated procedure for finding optimal quantum embeddings architecture that leads to high representation learning ability on the quantum Hilbert space. The algorithm is accessible and promising compared to the classical machine learning model, which can be implemented on near-term quantum computers. Although our QES cannot guarantee to find the optimal global design of the quantum embedding architecture in the full search space, the algorithm can discover high-performed architecture solutions under the constrain of the entanglement level.

REFERENCES

- [1] H.-Y. Huang, M. Broughton, M. Mohseni, R. Babbush, S. Boixo, H. Neven, and J. R. McClean, "Power of data in quantum machine learning," *Nature communications*, vol. 12, no. 1, pp. 1–9, 2021.
- [2] M. Schuld, "Supervised quantum machine learning models are kernel methods," *arXiv preprint arXiv:2101.11020*, 2021.
- [3] V. Havlíček, A. D. Córcoles, K. Temme, A. W. Harrow, A. Kandala, J. M. Chow, and J. M. Gambetta, "Supervised learning with quantum-enhanced feature spaces," *Nature*, vol. 567, no. 7747, pp. 209–212, 2019.
- [4] M. Schuld and N. Killoran, "Quantum machine learning in feature hilbert spaces," *Physical review letters*, vol. 122, no. 4, p. 040504, 2019.
- [5] S. Lloyd, M. Schuld, A. Ijaz, J. Izaac, and N. Killoran, "Quantum embeddings for machine learning," *arXiv preprint arXiv:2001.03622*, 2020.
- [6] M. Benedetti, E. Lloyd, S. Sack, and M. Fiorentini, "Parameterized quantum circuits as machine learning models," *Quantum Science and Technology*, vol. 4, no. 4, p. 043001, 2019.
- [7] E. Farhi and H. Neven, "Classification with quantum neural networks on near term processors," *arXiv preprint arXiv:1802.06002*, 2018.
- [8] J. R. McClean, S. Boixo, V. N. Smelyanskiy, R. Babbush, and H. Neven, "Barren plateaus in quantum neural network training landscapes," *Nature communications*, vol. 9, no. 1, pp. 1–6, 2018.
- [9] J. Romero and A. Aspuru-Guzik, "Variational quantum generators: Generative adversarial quantum machine learning for continuous distributions," *Advanced Quantum Technologies*, vol. 4, no. 1, p. 2000003, 2021.
- [10] J. R. McClean, J. Romero, R. Babbush, and A. Aspuru-Guzik, "The theory of variational hybrid quantum-classical algorithms," *New Journal of Physics*, vol. 18, no. 2, p. 023023, 2016.
- [11] J. Bergstra, R. Bardenet, Y. Bengio, and B. Kégl, "Algorithms for hyperparameter optimization," vol. 24, 2011.
- [12] R. A. Fisher, "The use of multiple measurements in taxonomic problems," *Annals of eugenics*, vol. 7, no. 2, pp. 179–188, 1936.
- [13] B. Zoph and Q. V. Le, "Neural architecture search with reinforcement learning," *arXiv preprint arXiv:1611.01578*, 2016.
- [14] B. Zoph, V. Vasudevan, J. Shlens, and Q. V. Le, "Learning transferable architectures for scalable image recognition," in *Proceedings of the IEEE conference on computer vision and pattern recognition*, 2018, pp. 8697–8710.
- [15] J. Bergstra and Y. Bengio, "Random search for hyper-parameter optimization," *Journal of machine learning research*, vol. 13, no. 2, 2012.
- [16] J. Snoek, H. Larochelle, and R. P. Adams, "Practical bayesian optimization of machine learning algorithms," *arXiv preprint arXiv:1206.2944*, 2012.
- [17] E. Real, A. Aggarwal, Y. Huang, and Q. V. Le, "Regularized evolution for image classifier architecture search," in *Proceedings of the aaai conference on artificial intelligence*, vol. 33, no. 01, 2019, pp. 4780–4789.
- [18] H. Liu, K. Simonyan, and Y. Yang, "Darts: Differentiable architecture search," *arXiv preprint arXiv:1806.09055*, 2018.

- [19] C. Liu, B. Zoph, M. Neumann, J. Shlens, W. Hua, L.-J. Li, L. Fei-Fei, A. Yuille, J. Huang, and K. Murphy, “Progressive neural architecture search,” in *Proceedings of the European conference on computer vision (ECCV)*, 2018, pp. 19–34.
- [20] N. Nguyen and J. M. Chang, “Contrastive self-supervised neural architecture search,” *arXiv preprint arXiv:2102.10557*, 2021.
- [21] T. Fösel, M. Y. Niu, F. Marquardt, and L. Li, “Quantum circuit optimization with deep reinforcement learning,” *arXiv preprint arXiv:2103.07585*, 2021.
- [22] N. Liu and P. Rebentrost, “Quantum machine learning for quantum anomaly detection,” *Physical Review A*, vol. 97, no. 4, p. 042315, 2018.
- [23] X. Gao, Z.-Y. Zhang, and L.-M. Duan, “A quantum machine learning algorithm based on generative models,” *Science advances*, vol. 4, no. 12, p. eaat9004, 2018.
- [24] V. Dunjko, J. M. Taylor, and H. J. Briegel, “Quantum-enhanced machine learning,” *Physical review letters*, vol. 117, no. 13, p. 130501, 2016.
- [25] O. A. Von Lilienfeld, “Quantum machine learning in chemical compound space,” *Angewandte Chemie International Edition*, vol. 57, no. 16, pp. 4164–4169, 2018.
- [26] S. Lloyd, S. Garnerone, and P. Zanardi, “Quantum algorithms for topological and geometric analysis of data,” *Nature communications*, vol. 7, no. 1, pp. 1–7, 2016.
- [27] S. Lloyd, M. Mohseni, and P. Rebentrost, “Quantum principal component analysis,” *Nature Physics*, vol. 10, no. 9, pp. 631–633, 2014.
- [28] E. Farhi, J. Goldstone, and S. Gutmann, “A quantum approximate optimization algorithm,” *arXiv preprint arXiv:1411.4028*, 2014.
- [29] A. Mari, T. R. Bromley, J. Izaac, M. Schuld, and N. Killoran, “Transfer learning in hybrid classical-quantum neural networks,” *Quantum*, vol. 4, p. 340, 2020.
- [30] W. Cappelletti, R. Erbanni, and J. Keller, “Polyadic quantum classifier,” in *2020 IEEE International Conference on Quantum Computing and Engineering (QCE)*. IEEE, 2020, pp. 22–29.
- [31] J. Romero, J. P. Olson, and A. Aspuru-Guzik, “Quantum autoencoders for efficient compression of quantum data,” *Quantum Science and Technology*, vol. 2, no. 4, p. 045001, 2017.
- [32] M. Schuld, A. Bocharov, K. M. Svore, and N. Wiebe, “Circuit-centric quantum classifiers,” *Physical Review A*, vol. 101, no. 3, p. 032308, 2020.
- [33] D. Shepherd and M. J. Bremner, “Instantaneous quantum computation,” *arXiv preprint arXiv:0809.0847*, 2008.
- [34] Č. Brukner, J.-W. Pan, C. Simon, G. Weihs, and A. Zeilinger, “Probabilistic instantaneous quantum computation,” *Physical Review A*, vol. 67, no. 3, p. 034304, 2003.
- [35] J. M. Arrazola, P. Rebentrost, and C. Weedbrook, “Quantum supremacy and high-dimensional integration,” *arXiv preprint arXiv:1712.07288*, 2017.
- [36] N. Killoran, T. R. Bromley, J. M. Arrazola, M. Schuld, N. Quesada, and S. Lloyd, “Continuous-variable quantum neural networks,” *Physical Review Research*, vol. 1, no. 3, p. 033063, 2019.
- [37] G. R. Steinbrecher, J. P. Olson, D. Englund, and J. Carolan, “Quantum optical neural networks,” *npj Quantum Information*, vol. 5, no. 1, pp. 1–9, 2019.
- [38] G. Verdon, M. Broughton, and J. Biamonte, “A quantum algorithm to train neural networks using low-depth circuits,” *arXiv preprint arXiv:1712.05304*, 2017.
- [39] M. Fingerhuth, T. Babej *et al.*, “A quantum alternating operator ansatz with hard and soft constraints for lattice protein folding,” *arXiv preprint arXiv:1810.13411*, 2018.
- [40] W. Huggins, P. Patil, B. Mitchell, K. B. Whaley, and E. M. Stoudenmire, “Towards quantum machine learning with tensor networks,” *Quantum Science and Technology*, vol. 4, no. 2, p. 024001, 2019.
- [41] Y. Du, M. Hsieh, T. Liu, and D. Tao, “The expressive power of parameterized quantum circuits,” *arXiv preprint arXiv:1810.11922*, 2018.
- [42] S. Lloyd, “Quantum approximate optimization is computationally universal,” *arXiv preprint arXiv:1812.11075*, 2018.
- [43] M. Cerezo, A. Sone, T. Volkoff, L. Cincio, and P. J. Coles, “Cost-function-dependent barren plateaus in shallow quantum neural networks,” *arXiv preprint arXiv:2001.00550*, 2020.
- [44] Y. Bengio, A. Courville, and P. Vincent, “Representation learning: A review and new perspectives,” *IEEE transactions on pattern analysis and machine intelligence*, vol. 35, no. 8, pp. 1798–1828, 2013.
- [45] I. Misra and L. v. d. Maaten, “Self-supervised learning of pretext-invariant representations,” in *Proceedings of the IEEE/CVF Conference on Computer Vision and Pattern Recognition*, 2020, pp. 6707–6717.
- [46] T. Chen, S. Kornblith, M. Norouzi, and G. Hinton, “A simple framework for contrastive learning of visual representations,” in *International conference on machine learning*. PMLR, 2020, pp. 1597–1607.
- [47] B. E. Boser, I. M. Guyon, and V. N. Vapnik, “A training algorithm for optimal margin classifiers,” in *Proceedings of the 5th Annual ACM Workshop on Computational Learning Theory*, pp. 144–152.
- [48] T. Chen, T. He, M. Benesty, V. Khotilovich, Y. Tang, H. Cho *et al.*, “Xgboost: extreme gradient boosting,” *R package version 0.4-2*, vol. 1, no. 4, 2015.
- [49] T. Elsken, J. H. Metzen, F. Hutter *et al.*, “Neural architecture search: A survey,” *J. Mach. Learn. Res.*, vol. 20, no. 55, pp. 1–21, 2019.
- [50] P. Ren, Y. Xiao, X. Chang, P.-Y. Huang, Z. Li, X. Chen, and X. Wang, “A comprehensive survey of neural architecture search: Challenges and solutions,” *arXiv preprint arXiv:2006.02903*, 2020.

APPENDIX

6.1 Experimental Environment and Setting

Our experiments are conducted using PennyLane and Qiskit quantum simulators in Python 3.6 and Pytorch 1.8. The implementation of search strategies is via Optuna 2.7.0 package. In the all experiments, we use Adam optimizer with initial learning rate of 0.5 and $\beta = (0.9, 0.999)$. The decay rate of the learning rate is set at 0.97 with a decay period of every 2 epoch. We train each architecture candidate for 100 and 50 epochs on synthesis and Iris datasets, respectively. Final validation accuracy of synthesis datasets based on five independent runs, while ten independent runs are used in the Iris dataset. Regarding the parameter setting for the TPE sampler, we initialize the search phase with 20 random trials, followed by 300 trials. The number of samples to evaluate the expected improvement each trial is 1000 samples. Moreover, the same number of trials is used for the random search sampler.

6.2 Analysis of Preliminary Experiments

Layout 1	Layout 2	Layout 3
0.1965	0.1341	0.1846
0.1793	0.1846	0.2011
0.1513	0.1184	0.2035
0.1984	0.1004	0.2151
0.1765	0.1048	0.2192

TABLE 2: The validation loss of preliminary quantum embedding layouts on Iris dataset. The same hyper-parameter setting is used across all experiments.

In the preliminary experiment on the Iris dataset, we hand-crafted layouts of entanglements for observations. We start with sampling a quantum embedding with an entanglement level of $k = 3$ to identify the first layout. Then we permute the order of CNOT gates to get the second layout. Finally, the last layout is constructed by adding a random CNOT gate to the second layout. The validation loss of each layout is reported in Table 2, which involves five independent runs. Let denote the actual means of the validation score as μ_1 , μ_2 , and μ_3 for corresponding layouts. The p-value for the t-test of the null hypothesis $H_0 : \mu_1 = \mu_2$ is 0.017. Thus, we have strong statistical evidence to reject the null hypothesis, meaning the two means are not equal. Similarly, the p-value of the t-test over null hypothesis $H_0 : \mu_2 = \mu_3$ is 0.001, indicating that there are differences in the mean validation loss from different quantum embedding architectures.